EBioMedicine 58 (2020) 102902

Contents lists available at ScienceDirect

EBioMedicine

journal homepage: www.elsevier.com/locate/ebiom

Research paper

Real-time imaging of polymersome nanoparticles in zebrafish embryos engrafted with melanoma cancer cells: Localization, toxicity and treatment analysis

Agnese Kocere[a,1], Julien Resseguier[a,1], Jens Wohlmann[a], Frode Miltzow Skjeldal[a], Shanawaz Khan[a], Martin Speth[a], Nils-Jørgen Knudsen Dal[a], Matthew Yoke Wui Ng[b], Noelia Alonso-Rodriguez[a], Edoardo Scarpa[c], Loris Rizzello[d,e], Giuseppe Battaglia[c,e,f,g], Gareth Griffiths[a], Federico Fenaroli[a,*]

[a] University of Oslo, Department of Biosciences, Blindernveien 31, 0371 Oslo, Norway
[b] University of Oslo, Domus Medica, Sognsvannsveien 9, 0317 Oslo, Norway
[c] University College London, Department of Chemistry, 20 Gordon Street, WC1H 0AJ London, United Kingdom
[d] University of Milan, Department of Pharmaceutical Sciences, via Mangiagalli 25, 20133 Milan (Italy)
[e] Institute for Bioengineering of Catalonia (IBEC), The Barcelona Institute of Science and Technology, Baldiri Reixac 10-12, 08028 Barcelona (Spain)
[f] Institute for the Physics of Living Systems, University College London, Gower Street, London, WC1E 6BT, London, United Kingdom
[g] Catalan Institution for Research and Advanced Studies (ICREA), Passeig Lluís Companys 2308010 Barcelona, Spain

ARTICLE INFO

Article History:
Received 4 January 2020
Revised 29 June 2020
Accepted 3 July 2020
Available online 21 July 2020

ABSTRACT

Background: The developing zebrafish is an emerging tool in nanomedicine, allowing non-invasive live imaging of the whole animal at higher resolution than is possible in the more commonly used mouse models. In addition, several transgenic fish lines are available endowed with selected cell types expressing fluorescent proteins; this allows nanoparticles to be visualized together with host cells.
Methods: Here, we introduce the zebrafish neural tube as a robust injection site for cancer cells, excellently suited for high resolution imaging. We use light and electron microscopy to evaluate cancer growth and to follow the fate of intravenously injected nanoparticles.
Findings: Fluorescently labelled mouse melanoma B16 cells, when injected into this structure proliferated rapidly and stimulated angiogenesis of new vessels. In addition, macrophages, but not neutrophils, selectively accumulated in the tumour region. When injected intravenously, nanoparticles made of Cy5-labelled poly(ethylene glycol)-block-poly(2-(diisopropyl amino) ethyl methacrylate) (PEG-PDPA) selectively accumulated in the neural tube cancer region and were seen in individual cancer cells and tumour associated macrophages. Moreover, when doxorubicin was released from PEG-PDPA, in a pH dependant manner, these nanoparticles could strongly reduce toxicity and improve the treatment outcome compared to the free drug in zebrafish xenotransplanted with mouse melanoma B16 or human derived melanoma cells.
Interpretation: The zebrafish has the potential of becoming an important intermediate step, before the mouse model, for testing nanomedicines against patient-derived cancer cells.
Funding: We received funding from the Norwegian research council and the Norwegian cancer society

1. Introduction

The treatment of cancer is one of the greatest challenges in modern medicine. While the therapeutic success rate for this group of diseases is generally improving, the number of cancer deaths is projected to increase 50% by 2040 due to an ageing global population [1]. Moreover, the common treatment using chemotherapy is known to cause severe toxicity for the patient, due to the side effects of the administered drugs. The main reason for this is that the drugs, when administered parenterally, reach all parts of the body, causing the well-known secondary effects such as nausea, fatigue and hair loss; importantly, these are conditions that restrict the volumes of given drug doses. In this respect, nanoparticles (NP) containing anti-cancer

* Corresponding author.
E-mail address: federico.fenaroli@ibv.uio.no (F. Fenaroli).
[1] Agnese Kocere and Julien Resseguier have contributed equally to this manuscript.

https://doi.org/10.1016/j.ebiom.2020.102902

Research in context

Evidence before this study

A number of groups have investigated the efficacy of anticancer drugs in free form in zebrafish embryos xenotransplanted with human or mice cancer cells. In most cases, the drugs were added to the fish bathing water, making it difficult to control the effective dose that enters the fish. For cancer chemotherapy, intravenously injected nano-sized carriers containing drugs represent a rapidly developing strategy. Until now, only a few studies have addressed the therapy of intravenously injected nanoparticles in tumour-bearing zebrafish embryos.

Added value of this study

Here, we introduce the zebrafish for visualizing and evaluating the efficacy of anti-cancer drug loaded nanoparticles. We injected cancer cells into the neural tube, a transplantation site which is better suited for tumour development and for light and electron microscopy imaging. In this system we followed the fate of intravenously injected nanoparticles. Our results reveal the zebrafish embryo to be a rapid and powerful screening tool to assess key parameters of nanoparticles aimed for cancer therapy namely: the toxicity, the localization and the treatment.

Implication of the available evidence

Our study opens the way for assessing the efficacy of drug-loaded nanoparticles on xenotransplants of patient-derived cancer cells. For this purpose the zebrafish embryo is unique in allowing an assessment in only 10 days and therefore seems to be very attractive for rapid analysis to select the most powerful formulations for pre-clinical characterization.

drugs have been studied for decades for their potential to reduce toxicity, due to their ability to protect the drug cargo and selectively target part of the injected dose to the diseased site. However, despite the success of some formulations, only about ten have been approved in Europe and US for human treatment until now [2].

The most commonly used preclinical animal model to study nanoparticles in the context of cancer is the mouse; in the majority of studies these rodents are transplanted with cancer cells derived from mice or humans [3]. A first disadvantage of this mammalian model is the need for immunocompromised mice to avoid their adaptive immunity rejecting the introduced cancer cells. Moreover, because of their opacity for imaging, high resolution analysis of NP accumulation in the diseased site in live mice is both limited and, when possible, complicated to perform. Possibilities to observe NP at high resolution include the use of 2-photon microscopy (for superficial tumours at a depth less than 200 μm); alternatively, the tumour can be exposed surgically, for example by skin flaps where a subcutaneous tumour is cut and the skin is exposed to the microscope lens. As another option, it is possible to create imaging glass windows for microscopy, which are inserted at the imaging sites to reach deeper tissues. These latter techniques have indeed been used by a handful of groups who have tried to visualize details of NP accumulation at tumour sites [4,5]. However, these methods do not allow imaging of the whole animal and require extremely skilled specialists, both for imaging and, in some instances, for building in house 2-photon microscope systems [6]. For these reasons, the vast majority of mouse cancer studies utilize the in vivo imaging tools such as In Vivo Imaging System (IVIS), which allows a resolution of only about 20 μm (according to the manufacturer) but has the advantage of being done at the whole animal level.

An alternative vertebrate animal model that is growing in popularity is the zebrafish. In its embryonic and larval stages, this fish possesses enormous advantages for imaging thanks to its transparency and the absence (until 3–6 weeks) of adaptive immunity, which allows the xenotransplanted cancer cells to avoid being rejected [7,8]. Besides the fact that detailed microscopy of the cancer cells can be easily performed at the whole animal level, an additional advantage of this vertebrate system is that this imaging can be combined with the availability of transgenic fish having fluorescently labelled specific cell types, such as endothelial cells or macrophages. This has allowed researchers to view the fate of the cancer cells in the context of important host cells that interact with them [9-11].

Using this system, several groups could introduce into the embryo different cancer cell types from humans, mice or from the zebrafish itself [10,12–14]. Given the lack of some orthotopic sites present in humans (e.g. lungs, breast, prostate) an important technical issue is the choice of region in the embryo where one can inject the foreign cells. For each potential injection site there are advantages and disadvantages. For simplicity of injection most groups [10,12,15–17] have transplanted cancer cells into the yolk sac or in the neighbouring perivitelline space; the yolk sac offers the largest volume in thickest areas of the embryo (about 0.5 mm) and therefore less convenient to image at high resolution. A few groups have instead injected cancer cells into selected blood vessels where they have a tendency to mechanically stop in the caudal hematopoietic tissue, a region only a few tens of microns thick and therefore especially suitable for imaging [18]. In our first publication on this topic we chose the latter approach by injecting different cancer cells in the heart cavity of the embryo but we faced the problem that the injected cells grew and proliferated very poorly and did not trigger local angiogenesis nor accumulation of leukocytes [9].

In the present study we chose a different approach by starting with a different cell type, mouse melanoma B16 cells, which have been previously shown to grow very well in the zebrafish [19]. We combined these with a different transplantation location, the developing neural tube. This injection site was introduced for studying tuberculosis (TB) granulomas using the fish TB organism *Mycobacterium marinum* by the group of Tobin [20] and subsequently used by our group [21] because of its clear advantages for imaging purposes, especially for visualizing neovascularization events. We show here how a few B16 cells transplanted in the neural tube grow and proliferate into a large and dense tumour mass within a week. This tumour-like aggregate stimulates angiogenesis and recruits tumour associated macrophages. Moreover, using pH-sensitive poly(ethylene glycol)-block-poly(2-(diisopropyl amino) ethyl methacrylate) (PEG-PDPA) polymersomes containing either a fluorescent dye or doxorubicin, we reveal that after intravenous injection this system is well-suited to evaluate drug toxicity, quantify NP accumulation at the tumour site and assess its therapeutic potential.

2. Methods

2.1. Nanoparticle preparation and characterization

2.1.1. Materials

All PEO starting materials were purchased from Iris Biotech. PEO-Br and N,-PEO-Br macroinitiators were synthesized according to the literature[22]. α-Bromoisobutyryl bromide (BIBB), triethylamine (TEA), 2-(diisopropylamino)ethyl methacrylate (DPA monomer), copper (I) bromide, bipyridin, copper sulfate, sodium ascorbate were purchased from Sigma Aldrich. Cy5-alkyne, and Cy7-alkyne were purchased from Lumiprobe. All solvents were purchased from Sigma Aldrich and used directly as provided unless specified.

2.1.2. Synthesis of PEO-b-PDPA block copolymers

PEO-b-PDPA and N_3-PEO-b-PDPA copolymers (for bioconjugations) were synthesized *via* atom-transfer radical polymerization (ATRP)[23]. Briefly, 0.2 mmoles (1 eq) of PEO macroinitiator were weighted in a round bottom flask fitted with a stirrer bar and a septum, and further dried under high vacuum for at least 30 min prior reaction. To this flask, 4 mL of isopropanol (previously degassed) were added and the solution was further purged with inert gas for at least 30 min. Next, 16 mmol (85 eq) of 2-(diisopropylamino)ethyl methacrylate (DPA monomer) in 2 mL of degassed isopropanol were added to the reaction flask. The complete mixture was purged under continuous anhydrous gas flow for another 30 mins. Finally, the reaction was set at 50 °C and the catalyst (Copper (I) bromide/bipyridin, 1 and 2 eq respectively) was quickly added as solid. The reaction was left under inert atmosphere, vigorous stirring at 50 °C for 24 h. For purification, the reaction was diluted with ethanol and left stirring at open air for 1 h The oxidised catalyst was easily removed by silica gel filtration in ethanol. Finally, the polymer was subsequently dialysed against chloroform/methanol 3:1 (v/v), then methanol and finally water to remove byproducts (MWCO depending on the PEO macroinitiator size). The final product was isolated via freeze-drying as an off-white solid. The identity, M_w and polydispersity of the lyophilised powder was analysed by NMR ($CDCl_3$) and GPC (water, pH = 2).

Synthesis of labelled PEO-b-PDPA copolymers (Cy5 labelled polymers)

One eq of N_3-PEO-b-PDPA was previously assembled in PBS by pH-switch procedure [24]. The solution of self-assembled polymer was then degassed by sonication and inert gas flow under stirring. The degassed solution was then mixed with 1.2 eq of Cy5-alkyne dissolved in degassed dimethylsulfoxide (DMSO), giving a final DMSO: PBS ratio of 10:1. Next, sodium ascorbate (5 eq) was added and the mixture was further degassed for at least 30 min. Finally, 1 eq of $CuSO_4$ was added under inert atmosphere and the reaction was left reacting at 40 °C for 72 h protected from light. Dialysis of the labelled polymers was done against DMSO and then water to purified them (MWCO at least 5 KDa for peptide purification and 3.5 KDa for dyes `purification). The labelled polymers were recovered after lyophilisation.

Polymersome production

PEO-PDPA block copolymer (18 mg) and Cy5-labelled PEO-PDPA block copolymer (2 mg) were dissolved in 900 μl of THF in a sterile glass vial containing a stir bar. For Doxorubicin encapsulation, 100 μl of a 1 mg/ml solution of doxorubicin hydrochloride (Sigma) dissolved in DMSO were added to the solution containing the dissolved block copolymers. Next, 2.3 mL of sterile phosphate buffer saline (PBS) pH 7.4 were added to the solution using a syringe pump (World Precision Instruments) set at a constant rate of 2 μl/minute at 40 °C under stirring. Following the completion of this process, further 3.7 mL of PBS were added and the solution was then extensively dialysed against an excess of PBS pH 7.4 (MWCO 3 KDa). Polymersome solutions were then centrifuged for 10′ at 1000 g, filtered through a size exclusion chromatography column of sepharose (Sigma) and concentrated using a hollow fibre module (750 kDa, Microkros). Final preparations were stored at 4 °C.

2.2. Zebrafish care and transgenic lines used

Zebrafish embryos were kept at 28.5 °C in petri dishes containing Zebrafish egg water supplemented with 0.003% phenythiourea (PTU). Throughout the experiments, in all conditions, a maximum of 20 zebrafish embryos were kept in each dish containing 20 ml of egg water. Zebrafish embryos were not fed after day 5. The zebrafish lines used were Tg(fli1a:EGFP) [25] for visualization of the vasculature, Tg (mpeg1:mcherry) [26] for visualization of macrophages and Tg(mpx: GFP) [27] for detection of neutrophils. All experiments were performed in accordance to the ethical standards and legislation for animal research in Norway (license FOTS id: 13563).

2.3. Cancer cells preparation for xenotransplantation

The B16F1 Mouse Melanoma Cancer cell line was received as a gift from Mælandsmo group at the Radium University Hospital, Oslo. The cells, transducted to express either GFP or RFP (via pGIPZ-RFP or pGIPZ-GFP lentiviral vectors), were grown at 37°C in RPMI1640 medium (Lonza) completed with 10% FBS (Saveen & Werner) and supplemented puromycin (Sigma-Aldrich, USA) at a final concentration of 2 μg/mL. For injection, the cells were prepared by detaching them using Versene (Life Technologies), centrifuged at 400 RCF which caused them to aggregate in a pellet. After a couple of washing cycles using Versene, the cells where filtered using a 70 μm cell strainer (VWR) and centrifuged once again. The supernatant was removed leaving a wet cell pellet, which was used to load glass needles for xenotransplantation. Human Melanoma, Melmet5 cancer cells expressing the fluorescence marker dsRed were handled as explained in our previous publication Evensen et al. [9].

2.4. Zebrafish injections

The glass needles necessary for injections are made of borosilicate (GC100T-10, Harvard Instruments) and were previously prepared using a pipette puller (P-97, Sutter Instruments). The needles, controlled *via* a Narishige MN-153 micromanipulator, are connected to an Eppendorf Femtojet Express pump which allows careful command of administered volumes. All the injections were performed on zebrafish larvae previously sedated with tricaine (Finquel; 0.02% in embryo water) and placed on a Petri dish containing a hardened solution of 2% agarose in Milli-Q water.

For Cancer cells injection, 100−150 B16 Mouse Melanoma cells were injected into the neural tube of zebrafish embryos three days post fertilization. This time point was chosen as, when the transplant is made on day 2, it is easier to obtain a disseminated foci along the neural tube rather than a solid tumour. After the cancer cell injection zebrafish embryos were kept at 32 °C, a temperature well tolerated by the developing animal.

For anticancer treatment, PEG-PDPA containing 2 mg/ml doxorubicin, free doxorubicin 2 mg/ml, empty NP or diluting medium were injected intravenously at four days post fertilization, 24 h after the transplants of cancer cells. Measurements on cancer cell growth (see below) were then made six days after anticancer treatment (seven days after transplant of cancer cells).

For NP visualization, PEG-PDPA containing Cy5 dye (5 mg/ml) were injected intravenously 7 days after B16 cancer cell xenotransplantation. After 8 h in circulations, images of zebrafish embryos were taken at with a Leica stereomicroscope (see below) or with a spinning disk Andor Dragonfly confocal microscope (see below).

2.5. Light microscopy

Zebrafish embryos were imaged at low resolution using a Leica DFC365FX stereomicroscope equipped with a 1.0 × planapo lens. This microscope, connected to fluorescent light, has been used for performing injections, for low magnification visualization of the zebrafish embryo and for performing different types of quantifications.

2.6. Cancer cells growth

Zebrafish embryos were injected Red fluorescent B16 Mouse Melanoma Cells in the neural tube. At different time points (3, 5 and 7 days) a picture at 30X using the Stereomicroscope was taken. The

value of fluorescence associated to the cancer cells was estimated using the free software Fiji.

2.7. Cancer cell growth following anticancer treatment or after macrophage ablation

Zebrafish embryos injected with either B16 mouse melanoma-RFP or Melmet5 human melanoma cancer cells-dsRed received treatments 24 h later as explained above. While zebrafish injected with B16 cells were kept at 32 °C, Melmet5 transplanted zebrafish were maintained at 35 °C. Seven days after the injection of cancer cells a picture at 30X using the Leica Stereomicroscope was taken for visualizing the fluorescence of the injected cells. The value of fluorescence associated to the cancer cells was estimated using the free software Fiji.

For macrophage ablation, the zebrafish line tg(mpeg1:Gal4FF; UAS:nfsB:mCherry) was used. This line expresses a nitroreductase in macrophages which in presence of metronidazole causes the selective apoptosis of macrophages. In this experiments we had two groups, one treated with Metronidazole dissolved in DMSO to reach a concentration of 3 mM in embryo water and another receiving only DMSO. The amount of DMSO for the two groups used was 0,15 ml in 100 ml of embryo water. Zebrafish were injected with GFP expressing B16 cancer cells at 72 h post fertilization and kept in water with or without metronidazole for 7 days. Evaluation of the cancer fluorescence was done using a stereomicroscope, as explained above.

2.8. Cancer cell proliferation and apoptosis following anticancer treatment

Zebrafish embryos injected with B16 mouse melanoma-GFP received treatments 24 h after cell xenotransplantas explained above. After six days, animals were anesthetized in buffered tricaine and place in a fixative solution (Formaldehyde 4% - HEPES 60 mM, pH7.4) for 24 h at room temperature. The fish were then dissected in fixative to remove the head and the tail in order to only keep the tumour-bearing region of the trunk. Following several rinses with PBS 1X and distilled water, samples were incubated 30 min in pre-chilled acetone at −20°C. Following additional rinses in PBS 1X and distilled water, the samples were permeabilized 1 h in PBS 1X complemented with 1% Triton X-100 (Sigma-Aldrich) (PBStx) at room temperature. Samples were saturated 3 h in a solution of Blockaid (Thermofisher) complemented with 1% Triton X-100 at room temperature. For the cancer cell proliferation analysis, samples were incubated overnight at room temperature with a rabbit anti-PCNA monoclonal antibody (ref 13,110 - Cell signalling) at a 1−200 dilution in PBSTx. For the cancer cell death analysis, samples were incubated overnight at room temperature with a rabbit anti-cleaved PARP polyclonal antibody (ref: 9541−Cell signalling) at a 1−200 dilution in PBSTx. Following 3 rinses of 1 h in PBSTx, samples were incubated overnight at 4°C in a mix of secondary goat anti-rabbit-Alexa647 (Jackson Immunoresearch) antibody at 1−250 dilution and DAPI at 1−200 dilution in PBSTx. Following three additional rinses in PBSTx and then PBS 1X, samples were mounted between coverslips using slowfade glass mounting medium (Thermofisher). Image acquisitions were made with the Zyla camera of a Dragonfly spinning disk confocal microscope (Andor), using 40 μm pin-holes and a 20x/0,75-dry objective. The images have been taken using 3D reconstructed tumors and using IMARIS software. The same program was used for quantification of the average PCNA and cPARP antibody staining within the tumour area. For PCNA staining, background subtraction was applied.

2.9. Endothelial cells growth

Transgenic zebrafish embryos having the vasculature labelled with GFP, Tg(fli1a:EGFP), were injected Red fluorescent B16 Mouse Melanoma Cells in the neural tube. At different time points (3, 5, 7 days) an image at 30X using the Stereomicroscope was taken to measure the green fluorescence. The value of fluorescence associated to the vasculature in the tumour area was estimated using the software Fiji. In this analysis, using a rectangle tool, the values represent fluorescence associated to the vasculature of the cancer region to which we subtracted the fluorescence of the vasculature in a healthy region of the same size. The measure of intersegmental vessels width has been performed using the program IMARIS on zebrafish embryos imaged with a spinning disk Andor Dragonfly confocal microscope (see below).

2.10. Macrophage and neutrophil accumulation in tumours

In this analysis transgenic zebrafish possessing fluorescent macrophages Tg(mpeg1:mcherry) or fluorescent neutrophils Tg(mpx:GFP) were xenotransplanted with B16 cancer cells. At day 7 the red fluorescence relative to macrophages or green fluorescence relative to neutrophils was quantified by taking a picture with the stereomicroscope and measuring the fluorescence intensity in the tumour region using the software Fiji.

2.11. Nanoparticle accumulation

In these experiments, Zebrafish embryos were injected with cancer cells at 72 h post fertilization. After 7 days, 5 nl of a solution of 10 mg/ml of NP was injected intravenously and 8 h later a picture of the zebrafish was taken. To quantify accumulation of NP, the fluorescence of NP in the tumour area was divided by the total NP fluorescence in the zebrafish. The values of fluorescence were obtained using the program Fiji.

2.12. High-resolution live-imaging

Zebrafish larvae were maintained under anaesthesia within a solution of buffered tricaine (120 μg/mL) and mounted, using low-melting agarose, onto the coverslip of a round-shaped petridish (MatTek). Acquisitions were made with the Zyla camera of a Dragonfly spinning disk confocal microscope (Andor), using 40 μm pin-holes and either a 10x/0,45-dry objective, a 20x/0,75-dry objective or a 60x/1,2-water objective. Acquisitions, stitches and deconvolutions were performed using the Fusion software. Image analysis was realized using IMARIS (version 9.51) and FIJI softwares (Imagej 1.51 g).

Fig. 2E was acquired using a Zeiss LSM 880 with Fast AiryScan using a LD LCI 63 × /1.2 objective with glycerol immersion.

2.13. Electron microscopy

Zebrafish injected with B16 mouse melanoma cancer cells were anaesthetised by placing them in 0.02% Tricane in embryo water. Subsequently the zebrafish were immersed in fixative (4% Formaldehyde FA, 0.8% Glutaraldehyde GA, 60 mM HEPES pH6.9 in embryo water) and immediately dissected (head and tail cut off with a razorblade) to facilitate fixative infiltration. Fixation was continued for 24 h at room temperature (RT) in about 500 μl fixative and another 24 h at 4 °C. Storage until further processing was in 60 mM HEPES 1% Formaldehyde FA at 4 °C up to several months. The samples were quenched in 100 mM glycine for 30 min at RT, embedded in a sheet of 12% bovine gelatine for protection and orientation using a sandwich of two coverslips and a spacers made from parafilm. The gelatine sandwich was solidified by cooling and immersion in 4% Formaldehyde FA in 60 mM HEPES pH 6.9 before the sample was cut out. For postfixation the sample was washed 3 times with freshly prepared 100 mM sodium bicarbonate buffer pH6.5 [HCl], incubated for 2 h on ice with 2% osmium tetroxide and 1.5% potassium ferricyanide in 100 mM sodium bicarbonate buffer pH6.5 [HCl], [28] washed

5 times 5 min with sodium bicarbonate buffer pH6.5 [HCl] and 2 times 5 min with 50 mM maleate buffer pH5.15 [NaOH] followed by 1 h incubation with 1% uranyl acetate in 50 mM maleate buffer pH5.15 [NaOH] [29] and 2 washes of 10 min with 50 mM maleate buffer pH5.15 [NaOH]. Storage overnight (approx. 10 h) was in 50 mM maleate buffer pH5.15 [NaOH]. Dehydration was performed by PLT [30] using dimethylformamide (DMF) [31] as a solvent, starting on ice with 30% DMF in water for 30 min, 50% DMF in water for 30 min on ice, 70% DMF in water for 30 min at −21 °C, 80% DMF in water for 40 min at −29 °C, 90% DMF in water for 40 min at −29 °C, 96% DMF in water for 60 min at −29 °C, two times 100% DMF for 60 min at −29 °C, 3 times 100% dry DMF for 30 min at −29 °C, 3 times 100% dry acetone for 30 min at −29 °C and finally 25% EPON in dry acetone at RT (about 25 °C) for approximately 10 h in an open vial on a rotating wheel under a fume hood. EPON [32] was prepared in a ratio of 3:7 (DDSA:NMA) and 1% DMP-30 fresh before use. The infiltration was continued using fresh 100% EPON for 24 h on a rotating wheel, the samples were embedded in flat embedding moulds and orientated after 3 h of polymerisation at 60 °C followed by incubation for 45 h at 60 °C and 24 h at RT (approx. 25 °C). After trimming and orientation the samples were sectioned at 60 nm thickness on a Leica UCT ultramicrotome using Diatome 45° ultra knifes and sections were mounted on carbon coated, formvar film on 1.5 × 2 mm copper slot grids. Imaging was performed on a Jeol JEM-1400 at 120 kV using a Tvips 216 camera. For montages, manually recorded Images were aligned using big stitcher in ImageJ and montaged using gimp for layer projection and photoshop CS6 coloration if applicable, generation of a tile pyramid and visualisation via java was done using OpenSeadragon and Openlayers on a basic html site.

2.14. Statistics used

Cancer cell growth in Fig 1F was analysed using a Brown-Forsythe and Welch ANOVA test. Angiogenesis progression in the tumour area of Fig 2F was analysed with a non-parametric Kruskal-Wallis test. Presence of macrophages and neutrophils in the cancer area in Fig 4F and G were analysed with an unpaired t-test with Welch correction. NP accumulation groups in Fig 5C were analysed with an unpaired t-test with Welch correction. Survival curves in Fig 6A were analysed using a Log-rank (Mantel-Cox) test. Treatment groups in Fig. 6B were analysed with a non-parametric Kolmogorov-Smirnov test. Fig 6G has been analysed with a non parametric unpaired t-test (Mann-Whitney test). Fig 6H and 6I have been analysed with an unpaired t-test with Welch correction. Normal distribution was analysed with the Anderson-Darling, D'agostino & Pearson and Shapiro-Wilk tests. Significance level is indicated as * for $P \leq 0.05$, ** for $P \leq 0.01$ and **** for $P \leq 0.001$. Throughout the manuscript, each zebrafish embryo has been used as an independent biological data point.

2.15. Author contributions

Agnese Kocere and Julien Resseguier carried out most of the experiments under the supervision of Federico Fenaroli and Gareth Griffiths. Jens Wohlmann performed the EM work. Martin Speth, Matthew Joke Wui Ng and Nils-Jørgen Knudsen Dal performed the transfections and selection of fluorescent cancer cells. Nils-Jøorgen Knudsen Dal and Noelia Alonso-Rodriguez carried out the experiments on human melanoma cancer cells and on tumour growth in presence or absence of macrophages. Shanawaz Khan performed the PCNA and PARP antibody staining. Frode Miltzow Skjeldal performed the data analysis on the PCNA and cPARP staining related images. Loris Rizzello and Edoardo Scarpa produced and characterized the DOX-loaded polymersomes. Giuseppe Battaglia designed the polymersomes backbone, provided guidelines on the assembly procedures and helped write the section on polymersome chemistry.

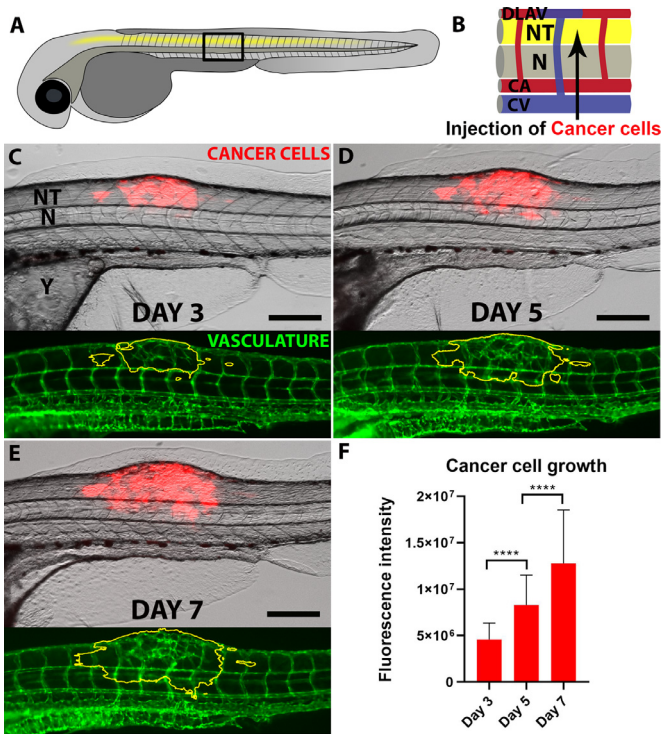

Fig. 1. B16 mouse melanoma cancer cells growth in the zebrafish neural tube.

A shows a schematic representation of the zebrafish embryo, with the trunk central region (black box) seen enlarged in B and showing the Neural Tube (NT), the Notochord (N) as well as the vessels named Dorsal Longitudinal Anastomotic Vessel (DLAV), Caudal artery (CA) and Caudal Vein (CV). A and B are adapted and modified from the original figure with permission from ACS Nano(21), Copyright (2018) American Chemical Society. The growth of mouse melanoma B16 cancer cells (red) following neural tube xenotransplantation is followed on days 3, 5 and 7 (C, D and E). Below each image it is possible to see the vasculature (green) which shows clear geometrical changes in the area of the tumour (yellow line). Quantification of cancer cells growth based on fluorescence is shown in F. For each time point, $N \geq 54$. Scale bars: 200 μm. Error bars indicate the Standard Deviation. Significance level is indicated as **** for $P \leq 0.0001$. (For interpretation of the references to colour in this figure legend, the reader is referred to the web version of this article.)

3. Results

3.1. Xenotransplanted B16 mouse melanoma cells thrive upon injection in the neural tube

At 72 h post-fertilization (hpf) we injected about 150−100 red fluorescent B16 mouse melanoma cells into the zebrafish neural tube (Fig 1A and B). Because the zebrafish embryo favors 28 °C while the injected cells prefer 37 °C we adopted an intermediate temperature of 32 °C at which the zebrafish were kept following the xenotransplant. Once injected in this region, these cells grew and proliferated very well, as is evident in Fig 1C-E. An EM image of B16 cancer cells in the neural tube 7 days after injection is presented in Supplementary Figure 1. The most common result of this type of injection is a single tumour locus while, in a restricted group of embryos, small disseminated cancer loci can be seen. This may happen because the neural tube is an extended tubular structure enclosing the developing spinal cord of the zebrafish and the injected cells can potentially be distributed all along this organ. A quantification based on total B16 cell fluorescence following the growth at days 3, 5 and 7 showed a linear increase in signal until the termination of the experiment (Fig. 1F). An EM micrograph showing a cancer cell dividing is shown in Supplementary Figure 2. Interestingly, mouse melanoma B16 cells often displayed striking protrusions. This feature can be better appreciated in Fig. 2B and E (see below).

3.2. Xenotransplanted cancer cells promote angiogenesis resulting in local loss of vascular organization

Another important feature of the xenotransplanted B16 cancer cells is their ability to stimulate angiogenesis [33]. This phenomenon is already evident at day 3 and this formation of new vessels continues until day 7 (lower images in Fig. 1C-E). In contrast, zebrafish injected with PBS in the neural tube did not show any growth of new vessels (Supplementary Fig 3 A-C). Protracted angiogenesis following the xenotransplant of B16 cancer cells results in the loss of geometry of the local vasculature (compared to the typical regular pattern seen in neighbouring non-injected areas) with a very chaotic network of new vessels that surround and crisscross the tumour. These new vessels (Fig. 2A and B) are often in the range of a few microns wide and appear to be active in blood flow since following intravenous injection of quantum dots or cyanin5 labelled PEG-PDPA the NP can be seen flowing in their lumen (Fig. 2C and Supplementary video 1). We quantified the width of the intersegmental vessels and observed that the ones in the tumour region are significantly thinner than the ones belonging to a healthy area (Supplementary Figure 3 D).

Angiogenesis associated with the tumours induced by xenotransplanted cancer cells is quite different from the one induced by fish tuberculosis Mycobacteria-dependant granuloma [20,21]. While the latter consists in enlarged intersegmental vessels and, less frequently the formation of new vessels, B16 cancer-induced angiogenesis results in complete loss of order, shrinkage of vessels and formation of several new vasculature branches (Fig. 2B and C). Importantly, injected B16 cancer cells seem to have an intimate connection with blood vessels (Fig. 2D, E, Supplementary Fig 4 and 5). Our confocal images show that these cells indeed not only are found in proximity to vessels but are seen in virtually every tumour to wrap around the endothelium. A quantification of the green fluorescence signal relative to newly growing endothelial cells (fli1a:GFP) in the cancer area shows a linear increase in green signal. Thus, as with the introduced cancer cells there is robust growth of the endogenous blood vessels adjacent to the tumour cell mass (Fig. 2F).

3.3. Xenotransplanted cancer cells are in direct contact with blood vessels as well as neural tube dendritic regions and basal lamina

In order to take a closer look at the interactions of the cancer cells with their microenvironment, we examined ultrathin sections of the neural tube by transmission electron microscopy (Fig 3A-C) in zebrafish injected with B16 cancer cells for a week. A version of Fig 3 that

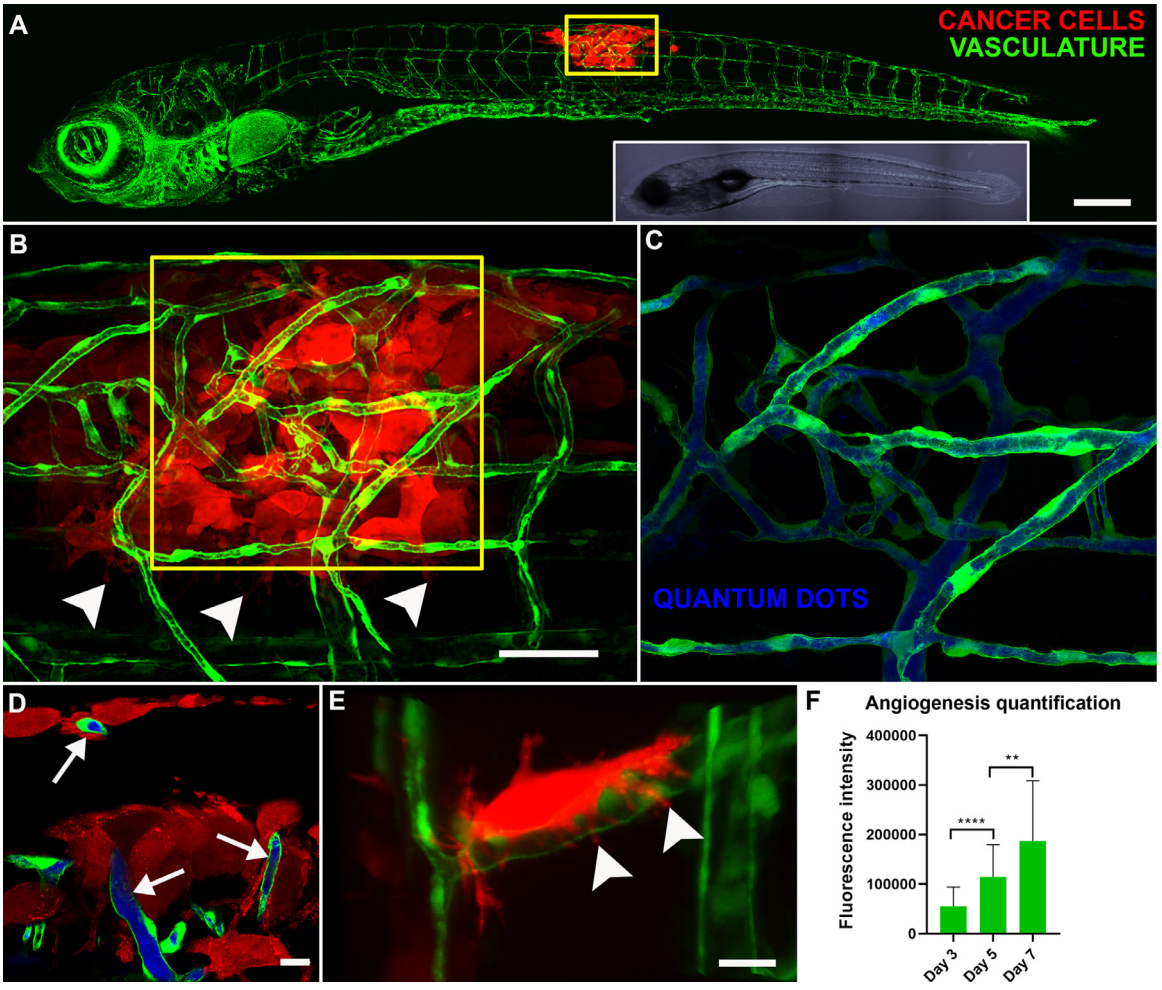

Fig. 2. Angiogenesis in the tumour area: Xenotransplantation of cancer cells (red) induce distinct changes in the local geometry of the vessels (green) that can be observed at the whole animal level (A). The inset shows the image of the zebrafish in the transmission channel. The tumour area in the yellow box in A is seen at higher magnification (B), yellow inset enlarged in (C) show flow of quantum dots (blue) in all newly formed vessels, showing that after their generation they are rapidly functional. Cancer cells appear to be tightly connected to endothelial cells in different sites as is evident in a thin stack of images (D) of the bigger tumour area (B). Cancer cells often appear to wrap around the vessels (E). Quantification of the total angiogenesis fluorescence in the area of the tumour based on fluorescence is shown in F. For each time point, $N \geq 53$. White arrowheads indicate cancer cells filopodia. White arrows indicate points of contact between cancer cells and endothelial cells. Scale bars: A, 200 μm; B, 50 μm; D, 10 μm and E 15 μm. Error bars indicate the standard deviation. Significance level is indicated as ** for $P \leq 0.01$ **** for $P \leq 0.001$. (For interpretation of the references to colour in this figure legend, the reader is referred to the web version of this article.)

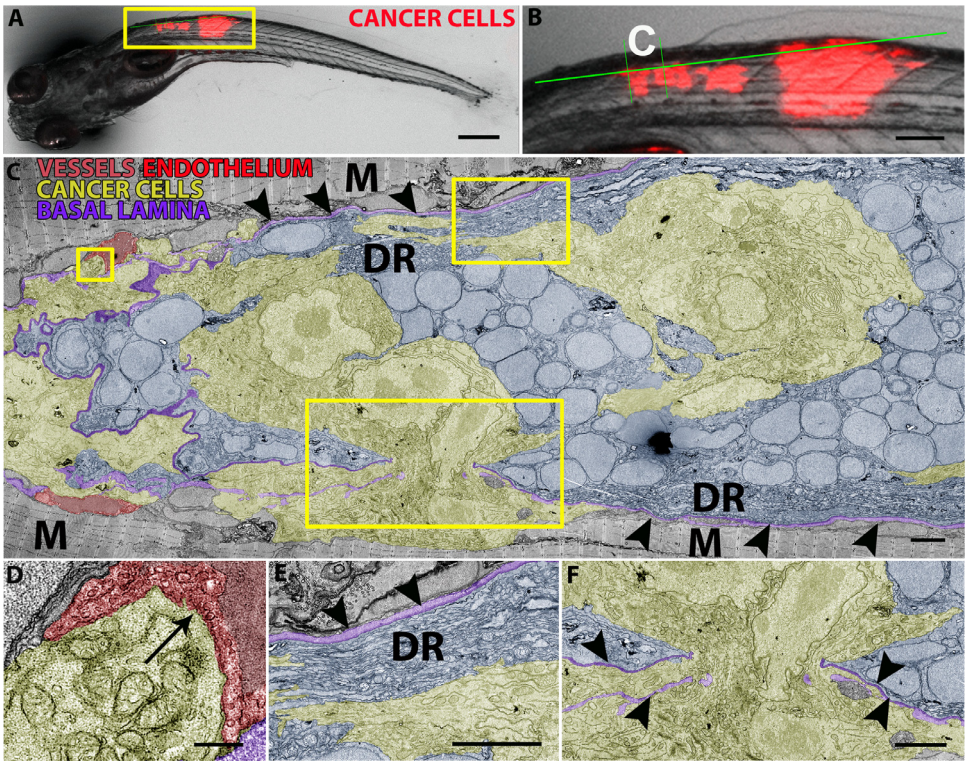

Fig. 3. Transmission EM of B16 cancer cells in the neural tube

A shows the xenotransplanted zebrafish embryo by light microscopy that was processed for EM. The area containing cancer cells (red, yellow box) is seen at higher magnification in B where we highlight the sectioning plane (long green line) while the area between the two shorter green lines is the region further visualized in C. In C, B16 mouse melanoma cancer cells (light yellow) are seen in the neural tube microenvironment (light blue) while in contact with blood vessels (light red), neural tube basal lamina (violet) and neural tube dendritic regions. Muscle, M; Dendritic region, DR. Top left yellow box of C is seen at higher magnification in D and shows direct contact (arrow) of a cancer cell with a blood vessel. Top middle yellow box in C is seen at higher magnification in E and shows the direct interaction of a cancer cell with a dendritic region of the neural tube. Bottom yellow box in C is seen at higher magnification in F and shows a cancer cell crossing the neural tube basal lamina. Arrowheads indicate the neural tube basal lamina.

Scale bars: A, 300 μm; B, 100 μm; C, 3 μm; 6, 500 nm; E-F, 3 μm. (For interpretation of the references to colour in this figure legend, the reader is referred to the web version of this article.)

allows one to zoom in and out at different magnifications is also available online at https://wohlmann.github.io/B16_MAP_H4c/. Cancer cells (light yellow) can easily be distinguished from the spinal cord precursor cells (light blue) due to their markedly different morphology and relatively large size. The xenotransplanted cells were almost invariably found to be located in proximity to blood vessels (light red, Fig 3C and 3D). Supporting Fig. 5, available also in a version where one can control the magnification is available at https://wohlmann.github.io/B16_MAP_F5c/, shows another clear example of cancer cells in the neural tube in direct contact with a blood vessel. Moreover B16 cancer cells were often seen interacting with neural tube dendritic regions (Fig 3E) and basal lamina (Fig 3F and Supplementary Fig 2). They also appeared to cross the basal lamina and could possibly interact with the extracellular spaces between muscles cells (Fig. 3F and Supplementary Fig 1).

3.4. Xenotransplanted tumours attract macrophages but not neutrophils

Tumours are often characterized by the presence of leukocytes, which play very important roles in the maintenance and development of cancer and are often regarded as one of the hallmarks of the disease [34]. Already from day 2 post-fertilization zebrafish embryos possess both neutrophils and macrophages [35], which are conveniently visualized using the fluorescent lines Tg(mpx:EGFP) and Tg (mpeg1:mcherry), respectively. We injected cancer cells and quantified the fluorescence relative to these two cells in the tumour, or a non-injected area. In the zebrafish embryo, macrophages were present in high numbers in the head region while only a few can normally be seen in the dorsal area where the neural tube lies. This makes it easier to appreciate after one week post-transplant that they clearly accumulate in the area where cancer cells are xenotransplanted; (Fig 4A, B and E). A quantification of the macrophage red fluorescence in this area shows that their presence is significantly higher in the tumour area relative to an equivalent site that had not received transplanted cancer cells (Fig 4F). In contrast, the number of neutrophils does not seem to be affected by the presence of the developing tumour; despite a slight trend of increased neutrophil fluorescence in the cancer area we could not detect a statistical difference compared to a site that was not injected with cancer cells (Fig 4C, D and G). By using the zebrafish line Tg(mpeg1:GAL4/UAS:NTR-mCherry) in which macrophages undergo apoptosis in presence of metronidazole we checked whether the growth of green fluorescent B16 cancer cells is influenced by the presence or absence of macrophages. Our results indicate mouse melanoma tumours grow slightly but significantly better when macrophages are absent (Supplementary Fig 6).

3.5. PEG-PDPA nanoparticles selectively accumulate in the cancer area

Having established that B16 cancer cells introduced into the neural tube are capable of a robust proliferation that stimulates local angiogenesis and local accumulation of tumour-associated macrophages, we were interested to see whether intravenously injected NP could accumulate in the cancer area. For this we injected B16 red fluorescent cancer cells into zebrafish embryos possessing green vasculature, tg(fli1a:EGFP) at day 3 post fertilization and injected intravenously (posterior caudal vein) PEG-PDPA NP (Size: 120 +/- 20 nm, PDI: 0.180) labelled with Cyanin 5 (far-red) on day 10 post fertilization (day 7 post transplant). Imaging of the injected zebrafish embryo

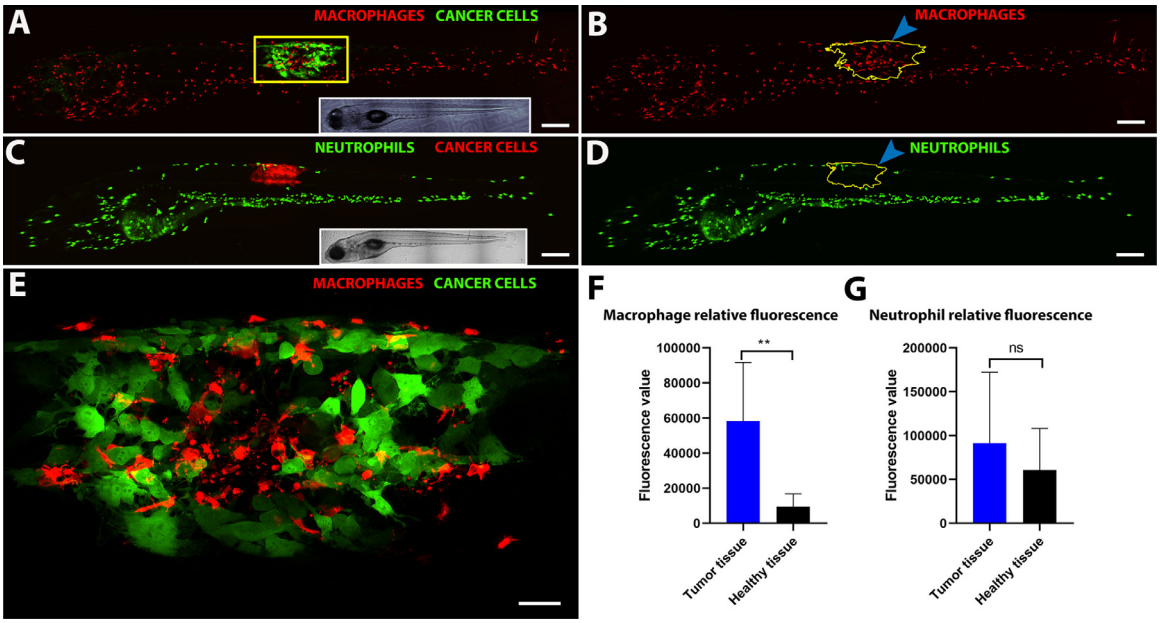

Fig. 4. Macrophages but not neutrophils are attracted to the tumour area

(A) Image at the whole animal level to show accumulation of macrophages (red) in the area of the tumour (green), a higher magnification of the tumour area (yellow rectangle in A) can be seen in E. The accumulation of macrophages in the cancer area (yellow outline) versus the surrounding tissues can be better appreciated in B. C shows images at the whole animal level of cancer cells (red) and neutrophils (green) while in D shows the same image with the periphery of the tumour outlined in yellow showing the similarity in neutrophil numbers between cancer area and healthy tissues. A quantification of total fluorescence associated with macrophage and neutrophils in the cancer area is shown in F and G, respectively. For each group of analysis, N is = 9. Scale Bars: A-D 150 μm. E 50 μm. In both A and B the insets show the image of the whole zebrafish embryo in the transmission channel. Error bars indicate the standard deviation. Significance level is indicated as ** for $P \leq 0.01$. (For interpretation of the references to colour in this figure legend, the reader is referred to the web version of this article.)

was performed 8 h later. NP accumulated selectively in the tumour area as is evident in Fig 5A, B and D. A quantification of the fluorescence in the cancer area confirmed that a significant amount of NP was found in the tumour area, when compared to an equivalent site in the neural tube of the zebrafish which was not injected with cancer cells (Fig 5C). The percentage of the total injected NP accumulating in the tumour mass was about 2%, and high resolution images of the NP in the cancer showed that a small amount of NP had indeed reached the cells and could be found inside them (Fig 5E). We then wondered whether macrophages would play a role for the increased accumulation in the tumour area of NP. For this we injected GFP-expressing cancer cells in zebrafish embryos having fluorescent macrophages tg(mpeg1:mcherry). After being 8 h in circulation cyanin5-labelled NP injected at day 7 post fertilization could be seen in the tumour region inside tumour-associated macrophages (Fig 5F, blue arrowheads).

3.6. *PEG-PDPA NP containing doxorubicin significantly reduce toxicity and improve cancer therapy*

PEG-PDPA NP is a promising NP formulation which consists of polymersomes that release their content only at low pH [36].This could for example facilitate release of the drug when the NP are degraded in lysosomes. We hypothesized that these NP encapsulating doxorubicin (dox) would show a significant reduction in systemic toxicity of the zebrafish embryo compared to the free drug. To test this hypothesis we compared dox-containing NP with the drug in free form; as controls we also injected empty NP and the injection medium alone (Fig. 6A). Our results show that toxicity of dox was reduced at least 40 fold when the drug was administered entrapped in PEG-PDPA NP. Indeed, intravenous injection of only 1 ng of injected free dox or 40 ng of dox encapsulated into PEG-PDPA resulted in about 70% survival of zebrafish embryos five days after the treatment. Both empty NP and the injection medium resulted in complete survival of the embryos, as did 10 or 20 ng dox entrapped into PEG-PDPA NP. Importantly, xenotransplants of mouse B16 cancer cells do not alter the survival of zebrafish embryos compared to PBS injected controls (Supplementary Fig 7).

Having established the potential of the dox-PEG-PDPA NP in reducing systemic toxicity in the zebrafish embryo compared to the free drug, we next addressed its therapeutic effect in our cancer model. For this, cancer cells were injected at day 3 post-fertilization while PEG-PDPA NP containing dox (40 ng) or free dox (1 ng) were intravenously administered 24 h later. As controls we also injected empty NP or the NP medium. At day 7 after xenotransplantation we measured the fluorescence of cancer cells in each group. Measurement of the relative cancer fluorescence revealed that the group injected with PEG-PDPA NP had significantly less fluorescence signal compared to the free doxorubicin and to the control groups with over 50% reduction of the cancer cell signal (Fig. 6B-F). We further characterized the different cancer treatments at day 7 after xenotransplant by analysing, on fixed zebrafish larvae, the tumour volume (Fig 6G) and the antibody labelling of markers for cancer cell proliferation, Proliferating Cell Nuclear Antigen (PCNA, Fig 6H) and apoptosis, poly(ADP-ribose) polymerase cleavage (cPARP, Fig 6I). Our results show that the Dox NP group was the one with the smallest tumour volumes, with significant differences compared to all the other groups. Moreover the Dox NP group had the lowest average cancer cell proliferation, showing a statistically significant reduction compared to the NP control group (Fig 6H). The same Dox NP group showed higher cancer cell death which is statistically significant compared to all other groups (Fig 6I). Images from each group of analysis are provided as Supplementary Fig 8.

Finally, in order to corroborate our analysis using human derived tumours, we performed a similar experiment using dsRed expressing human melanoma cancer cells, Melmet5 [37]. Our results showed that both NP-dox and free dox groups had fluorescence signals derived from the tumour that were significantly lower than the PBS injected control. No significant difference was found between NP-dox and free dox groups although the average in the free

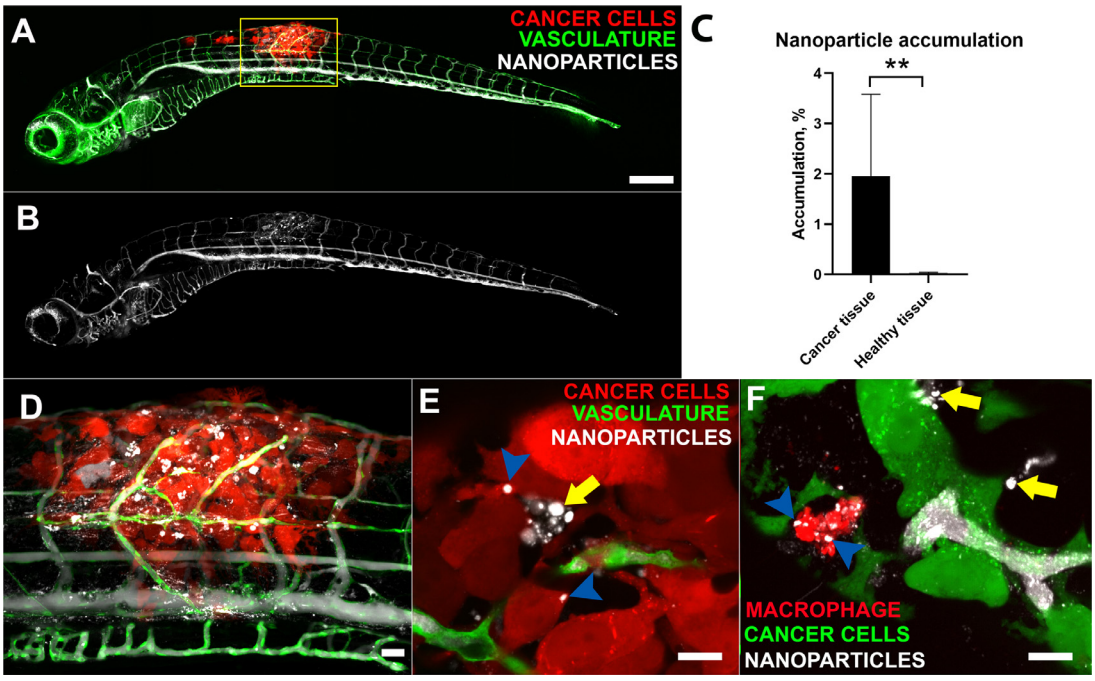

Fig. 5. Accumulation of PEG-PDPA NP in the area of the tumour.

In A, nanoparticles (white) injected intravenously can be seen flowing in vessels along the zebrafish (green) and selectively accumulate in the tumour area (red) The inset shows the image in the transmission channel. The same image is shown in B only in the NP channel to highlight the local accumulation. A quantification of NP accumulation based on fluorescence is shown in Fig. C. For both groups of analysis, $N = 13$. D shows higher magnification of the tumour area (yellow box in A). E shows two confocal slices in which the injected NP (white) appear to be inside cancer cells (red, blue arrowheads) while others are free in the intercellular spaces (yellow arrows). F shows a confocal stack in which it is visible a macrophage (red) near B16 cancer cells (green) having taken up NP (white, blue arrowheads). Other NP are free outside macrophages and in the vicinity of cancer cells (yellow arrows). Scale Bars: A-B, 200 μm, C, 50 μm, E and F 10 μm. Error bars indicate the standard deviation. Significance level is indicated as ** for $P \leq 0.01$. (For interpretation of the references to colour in this figure legend, the reader is referred to the web version of this article.)

dox group was about twelve percent higher than the NP-dox group (Supplementary Fig 9).

4. Discussion

After the initial physico-chemical characterization, current NP formulations evaluated for consideration as anti-cancer drugs are normally analysed first in cultured cells and, if promising, subsequently in a mouse model. The latter serves as the reference preclinical system before human testing. However, following this strategy only about 10 new nano-based formulations have been approved after 1996, the year that the first clinical NP, Doxil/Caelyx was introduced [2]. We argue that this disappointing success rate, at least in part, may be a consequence of the fact that the imaging possibilities in mouse are so limited. This is true both with respect to visualizing cancer cells and the cells with which they interact, and in monitoring the NP in order to be able to conclude that these NP have reached desirable or undesirable locations in the body.

The zebrafish model possesses key advantages over the mouse, making it a very attractive vertebrate model to represent the first stage of in vivo testing of NP. Consider the following practical advantages of the zebrafish system over the mouse: 1. *It is cheap*. The cost of using zebrafish embryos is low compared to the mouse; in fact at Boston university the cost of maintenance of one tank of twenty zebrafish was estimated to be less than a quarter of the price of a single mouse [38]. 2. *It is fast*. Zebrafish embryos are produced every day in aquaculture facilities and our experiments were all terminated by day 10 post-fertilization. In contrast, mouse experiments usually take several weeks. 3. *It is simple*. Parameters such as NP accumulation, NP toxicity and NP treatment can all be analysed without the need for complex and expensive microscopes; a conventional stereomicroscope equipped for fluorescence is often sufficient. 4. *It is precise*. A consequence of the superior imaging at the whole organism level is the ability one gets of quickly deciding whether or not any NP accumulate in sites considered undesirable; for example some NP have a tendency to attach to, and be taken up by the endothelial cells lining blood vessels; this a clearly unwanted outcome for treatment of most localized diseases. 5. *In the embryo there is no rejection of xenotransplanted cancer cells*. By lacking active adaptive immunity in the first weeks post-fertilization, the fish cannot identify the introduced cells as being foreign. 6. *Experiments are less ethically demanding.* The use of the zebrafish allows the replacement of mouse, in agreement with the guidelines of the 3R principles [39]. Many experiments such as testing free drugs and NP-encapsulated drugs for toxicity can be terminated before day 5 when the fish are still considered as embryos. Moreover, the ethical requirements after this period are much less challenging than those needed for mice; for example the number of animals permitted for an experiment is much higher for the fish than for the mouse; this facilitates more rigorous statistics 7. *It requires less volumes of NP and drugs*. Testing NP in the mouse usually requires about 100 microliters of NP formulation in each animal while for the zebrafish, a normal volume is 10 nanoliters, ten thousand times less. This is obviously an advantage for preliminary testing, especially when NP formulations contain expensive drugs. The obvious conclusion from all these facts is that the zebrafish embryo is extremely well-suited for precisely screening which NP formulations are worthy of more detailed testing in mouse and other mammalian models. An additional advantage of the zebrafish is the fact that about 70% of the human genes have a human orthologue [40]. Nevertheless, the zebrafish genome has undergone duplication and has multiple copies of several genes; this factor may complicate the studies of several diseases since duplications are evident also in genes related to immunity. Moreover

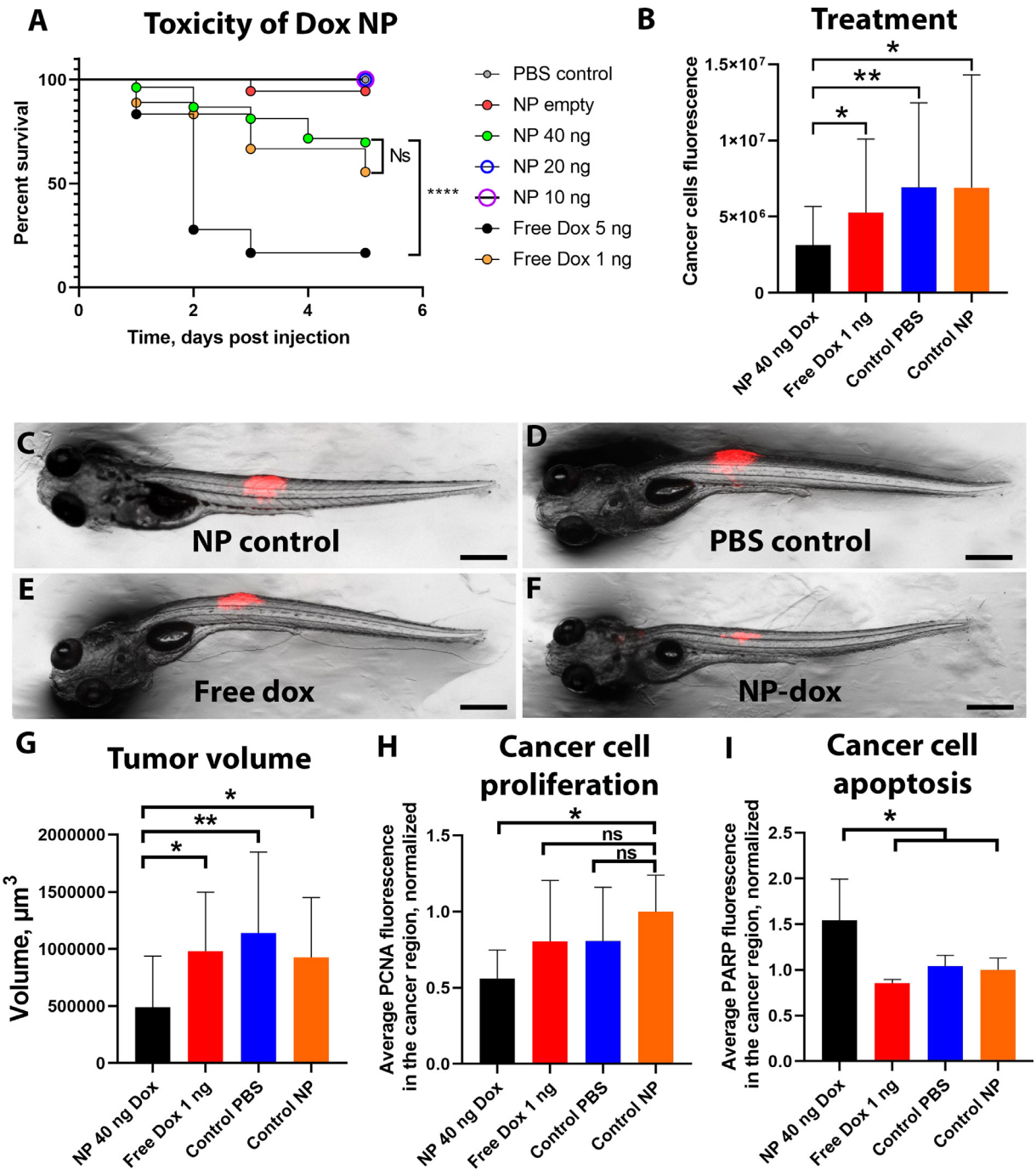

Fig. 6. PEG-PDPA-doxorubicin toxicity and cancer therapy.

A shows *via* an embryo survival graph the toxicity of PEG-PDPA-doxorubicin versus free doxorubicin. $N \geq 18$ in each group. B shows the measurements based on fluorescence of cancer cells growth at day 7 when zebrafish received either 40 ng of doxorubicin in PEG-PDPA NP or 1 ng of free doxorubicin, or were injected with NP control (without doxorubicin) or PBS. $N \geq 20$ in each group. Representative images of each group can be seen in C, D, E and F. G, H and I are graphs showing the quantification of tumour volume (G), cancer cell proliferation (PCNA antibody labelling, H) and cancer cell apoptosis (cPARP antibody labelling, I) of zebrafish receiving the four treatments, at seven days after xenotransplantation. In G, $N \geq 9$ in each group of analysis, in H, $N \geq 5$ in each group of analysis, in I, $N \geq 4$ in each group of analysis. The results are shown normalized to the control NP group. Scale bars: 300 μm. Error bars indicate the standard deviation.

Significance level is indicated as ** for $P \leq 0.01$ and * for $P \leq 0.05$, ns stands for not significant.

cytokines, although often similar in sequence, are largely incompatible between zebrafish and mammalian cells; this is an issue recently examined by Rajan and colleagues who have generated a humanized zebrafish expressing human hematopoietic-specific cytokines in order to promote survival and differentiation of human hematopoietic stem and progenitor cells [41].

The differences between zebrafish and the human genome, and cytokine incompatibility may have contributed to the difficulty of producing a cancer model in zebrafish such that it recapitulates important features of human cancer such as rapid growth, angiogenesis and presence of tumour-associated macrophages. To our knowledge, only Zhao and colleagues [19] had been able to show rapid and sustained growth and proliferation of xenotransplanted cancer cells in zebrafish. In addition, while no group had shown tumour accumulation of macrophages, the most cited paper describing angiogenesis following a xenotransplant in zebrafish embryos utilized a cell line

that was engineered to over-express the growth factor fibroblast growth factor (FGF) to artificially boost neovascularization [10]. Here, we chose the neural tube, the developing spinal cord of the zebrafish embryo as our site of injection in the absence of exogenous growth factors.

A number of researchers before us have attempted to inject cancer cells into neural tissue, notably a number of groups managed to successfully inject Glioblastoma cells into the hindbrain or midbrain of zebrafish embryos 2 or 3 days old. These type of injections are technically demanding and due to the delicate site of injection there is an increased risk to damage the developing zebrafish. Nevertheless some authors managed to show cancer growth in embryos and tested the effects on the tumours of drugs dissolved in the water [42,43]. Pudelko and colleagues used a different approach by injecting glioblastoma cells in the zebrafish blastomere at the early 1000 cell division stage. Strikingly, during development, cancer cells were found in both the mid- and hindbrain. This approach appear less invasive than brain injections and, due to the early stage transplantation, allows one to observe the development of orthotopic tumours [44].

The reason we chose the neural tube as transplant site is mainly due to its suitability for high resolution imaging and for the possibility of injecting a high number of cells with a minimum risk of affecting embryo development.

By using B16 mouse melanoma cells we show that, when injected in the neural tube, these cells grow quickly forming bulging tumours, promote local angiogenesis and exhibit an increased number of macrophages compared to neighbouring tissues. Electron microscopy images show that these cells, upon injection, make direct contact with blood vessel endothelium and are often seen crossing the neural tube basal lamina before invading the extracellular matrix between muscle cells.

Although our light and electron microscopy analysis clearly revealed that the cancer cells are in very close contact with the newly developed vasculature, we never witnessed any hint of metastasis and the cancer cells always remained confined in the neural tube or the neighbouring tissues. This observation is in sharp contrast with several reports in the literature claiming the metastatic potential of different cells lines tested in the zebrafish embryo [16,45,46]. However, all those studies were performed by injecting cancer cells into the yolk sac or perivitelline space which, because of their close proximity to major embryonal blood vessels, may not be the ideal site to test such hypotheses. Moreover, metastasis events were typically observed within a day after xenotransplant, a time insufficient for the injected cancer cells to form solid tumours or to tightly adhere to the surrounding tissues.

Despite the absence of metastasis the neural tube model is a robust system to visualize the growth and proliferation of the tumour mass as well as to follow angiogenesis and the accumulation of the macrophages. It is also an attractive system to follow the fate of injected NP relative to the tumour. We recently showed how the zebrafish can help in predicting the biodistribution of intravenously injected NP in mice [47]. The far red-labelled PEG-PDPA NP that we tested in our zebrafish cancer system accumulated in the tumour mass in a significant manner compared to neighbouring tissues; however they did so much less (about 2%) than in our zebrafish tuberculosis model system in which up to 20% of the injected NP could be found in the proximity of the *Mycobacterium marinum* granulomas [21]. By fluorescence microscopy, a small fraction of the injected NP could even be seen to be internalized by cancer cells and tumour-associated macrophages.

Prior to testing the anti-cancer potential of the NP containing doxorubicin we analysed another important parameter: their toxicity in comparison with the free compound. We and others have shown that the zebrafish embryo is exquisitely suited for this task [48-50]. Our results revealed a dramatic reduction of toxicity as 40 ng of drug loaded into NP was equivalent to 1 ng injected in free form. To put these values in a human perspective, the dose of doxorubicin given to an adult weighing about 60 kg and 1.7 mt tall is about 100 mg every 3 weeks, a dose of 1.7 mg/kg. In zebrafish, weighing approximately 1 mg, we have given a dose of 1 mg/kg of free drug (1 ng) and a much higher 40 mg/kg of NP-doxorubicin (40 ng). Given this promising result, we tested these NP for their potential to inhibit B16 cancer growth and showed that, six days after the treatment, cancer fluorescence was about 50% of the controls injected with PBS or treated with the free drug. Moreover they reduced cancer cell proliferation and significantly increased cancer cell apoptosis. We further tested our NP against a human melanoma line Melmet5 expressing the fluorescent reporter dsRed we observed six days after the treatment that the fluorescence relative to cancer cells in the NP-dox-treated group was significantly lower compared PBS control group and about 12% lower compared with that of zebrafish treated with free dox.

Only a few research groups have tried to test treatments with drugs or drug-NP conjugates after injection into the zebrafish embryo cancer models; almost all groups have added the drugs directly into the fish water. However, that approach is not an ideal method as the drug accumulation into the fish will be difficult to control and will be largely dependant on the uptake of the drug through the skin on the animal [15,51]. A prominent exception is the group of Spaink who injected the NP in the blood 5 h after intravenous injection of cancer cells. One day later the cancer cells were imaged and Coil/Coiled NP containing doxorubicin showed therapeutic promise in that they decreased the mass of cancer cells within the embryo [52].

5. Conclusion

We provide evidence that the zebrafish neural tube cancer model introduced here is a very promising vertebrate model for rapid screening of NP accumulation at the tumour site as well as NP-drug toxicity and therapeutic capability. The NP formulations showing the highest potential in this vertebrate model could then in future studies be further assessed in the mouse, the most common preclinical model. This type of approach could dramatically reduce the research time and costs associated with high numbers of mice. We therefore argue that the addition of this animal model would strengthen and facilitate the approval of new NP-based drugs for the treatment of cancer.

Authors' disclosure

All the authors declare that they have no conflict of interest.

Acknowledgments/Funding

We acknowledge the funding of the Norwegian cancer society (funding code: 206204) and Research Council Norway (funding codes: 273319, 275873). The funders had no role in the study design, data collection, data analysis, interpretation and writing of the report. We also want to thank the support of the IBV EM facility (head: Norbert Roos) and the imaging platform (head: Oddmund Bakke). We are especially grateful to the group of Gunhild Mælandsmo for sharing with us their B16F1 mouse melanoma and Melmet5 cancer cell line. We thank the group of Fahri Saatcioglu and in particular Hatice Zeynep Nenseth for providing the PCNA and cPARP antibodies.

Supplementary materials

Supplementary material associated with this article can be found, in the online version, at doi:10.1016/j.ebiom.2020.102902.

References

[1] Foreman KJ, Marquez N, Dolgert A, Fukutaki K, Fullman N, McGaughey M, et al. Forecasting life expectancy, years of life lost, and all-cause and cause-specific mortality for 250 causes of death: reference and alternative scenarios for 2016-40 for 195 countries and territories. Lancet 2018;392(10159):2052–90.

[2] Tran S, DeGiovanni PJ, Piel B, Rai P. Cancer nanomedicine: a review of recent success in drug delivery. Clin Transl Med 2017;6(1):44.

[3] Eswaraka J. Giddabasappa A. Chapter 6 - Humanized Mice and PDX Models. In: Uthamanthil R, Tinkey P, editors. Patient derived tumor xenograft models. Academic Press; 2017. p. 75–89.

[4] Matsumoto Y, Nichols JW, Toh K, Nomoto T, Cabral H, Miura Y, et al. Vascular bursts enhance permeability of tumour blood vessels and improve nanoparticle delivery. Nat Nanotechnol 2016;11(6):533–8.

[5] Miller MA, Chandra R, Cuccarese MF, Pfirschke C, Engblom C, Stapleton S, et al. Radiation therapy primes tumors for nanotherapeutic delivery via macrophage-mediated vascular bursts. Sci Transl Med 2017;9(392).

[6] Kim D, Kang J, Wang T, Ryu HG, Zuidema JM, Joo J, et al. Two-Photon In Vivo Imaging with Porous Silicon Nanoparticles. Adv Mater 2017;29(39).

[7] Lam SH, Chua HL, Gong Z, Lam TJ, Sin YM. Development and maturation of the immune system in zebrafish, Danio rerio: a gene expression profiling, in situ hybridization and immunological study. Dev Comp Immunol 2004;28(1):9–28.

[8] Langenau DM, Ferrando AA, Traver D, Kutok JL, Hezel J-PD, Kanki JP, et al. In vivo tracking of T cell development, ablation, and engraftment in transgenic zebrafish. Proc. Natl. Acad. Sci. U.S.A. 2004;101(19):7369.

[9] Evensen L, Johansen PL, Koster G, Zhu K, Herfindal L, Speth M, et al. Zebrafish as a model system for characterization of nanoparticles against cancer. Nanoscale 2016;8(2):862–77.

[10] Nicoli S, Ribatti D, Cotelli F, Presta M. Mammalian tumor xenografts induce neovascularization in zebrafish embryos. Cancer Res 2007;67(7):2927–31.

[11] Tulotta C, Stefanescu C, Chen Q, Torraca V, Meijer AH, Snaar-Jagalska BE. CXCR4 signaling regulates metastatic onset by controlling neutrophil motility and response to malignant cells. Sci Rep 2019;9(1):2399.

[12] Haldi M, Ton C, Seng WL, McGrath P. Human melanoma cells transplanted into zebrafish proliferate, migrate, produce melanin, form masses and stimulate angiogenesis in zebrafish. Angiogenesis 2006;9(3):139–51.

[13] Heilmann S, Ratnakumar K, Langdon E, Kansler E, Kim I, Campbell NR, et al. A quantitative system for studying metastasis using transparent zebrafish. Cancer Res 2015;75(20):4272–82.

[14] Lee LM, Seftor EA, Bonde G, Cornell RA, Hendrix MJ. The fate of human malignant melanoma cells transplanted into zebrafish embryos: assessment of migration and cell division in the absence of tumor formation. Dev Dyn 2005;233(4):1560–70.

[15] Fior R, Póvoa V, Mendes RV, Carvalho T, Gomes A, Figueiredo N, et al. Single-cell functional and chemosensitive profiling of combinatorial colorectal therapy in zebrafish xenografts. Proc Natl Acad Sci USA 2017;114(39):E8234–E43.

[16] Teng Y, Xie X, Walker S, White DT, Mumm JS, Cowell JK. Evaluating human cancer cell metastasis in zebrafish. BMC Cancer 2013;13:453.

[17] Yang X-J, Cui W, Gu A, Xu C, Yu S-C, Li T-T, et al. A novel zebrafish xenotransplantation model for study of glioma stem cell invasion. PLoS ONE 2013;8(4) e61801-e.

[18] Follain G, Osmani N, Azevedo AS, Allio G, Mercier L, Karreman MA, et al. Hemodynamic forces tune the arrest, adhesion, and extravasation of circulating tumor cells. Dev Cell 2018;45(1):33–52.

[19] Zhao C, Wang X, Zhao Y, Li Z, Lin S, Wei Y, et al. A novel xenograft model in zebrafish for high-resolution investigating dynamics of neovascularization in tumors. PLoS ONE 2011;6(7) e21768-e.

[20] Oehlers SH, Cronan MR, Scott NR, Thomas MI, Okuda KS, Walton EM, et al. Interception of host angiogenic signalling limits mycobacterial growth. Nature 2015;517(7536):612–5.

[21] Fenaroli F, Repnik U, Xu Y, Johann K, Van Herck S, Dey P, et al. Enhanced permeability and retention-like extravasation of nanoparticles from the vasculature into tuberculosis granulomas in zebrafish and mouse models. ACS Nano 2018;12(8):8646–61.

[22] Gaitzsch J, Appelhans D, Grafe D, Schwille P, Voit B. Photo-crosslinked and pH sensitive polymersomes for triggering the loading and release of cargo. Chem Commun (Camb) 2011;47(12):3466–8.

[23] Blanazs A, Massignani M, Battaglia G, Armes SP, Ryan AJ. Tailoring macromolecular expression at polymersome surfaces. Adv Funct Mater 2009;19(18):2906–14.

[24] Tian X, Nyberg S, P SS, Madsen J, Daneshpour N, Armes SP, et al. LRP-1-mediated intracellular antibody delivery to the Central Nervous System. Sci Rep 2015;5:11990.

[25] Lawson ND, Weinstein BM. In vivo imaging of embryonic vascular development using transgenic zebrafish. Dev Biol 2002;248(2):307–18.

[26] Ellett F, Pase L, Hayman JW, Andrianopoulos A, Lieschke GJ. mpeg1 promoter transgenes direct macrophage-lineage expression in zebrafish. Blood 2011;117(4):e49–56.

[27] Lieschke GJ, Oates AC, Crowhurst MO, Ward AC, Layton JE. Morphologic and functional characterization of granulocytes and macrophages in embryonic and adult zebrafish. Blood 2001;98(10):3087–96.

[28] Wood RL, Luft JH. The influence of buffer systems on fixation with osmium tetraoxide. J Ultrastruct Res 1965;12:22–45.

[29] Reese TS, Karnovsky MJ. Fine structural localization of a blood-brain barrier to exogenous peroxidase. J Cell Biol 1967;34(1):207–17.

[30] Carlemalm E, Villiger W, Hobot JA, Acetarin JD, Kellenberger E. Low temperature embedding with Lowicryl resins: two new formulations and some applications. J Microsc 1985;140(Pt 1):55–63.

[31] Meissner DH, Schwarz H. Improved cryoprotection and freeze-substitution of embryonic quail retina: a TEM study on ultrastructural preservation. J Electron Microsc Tech 1990;14(4):348–56.

[32] Luft JH. Improvements in epoxy resin embedding methods. J Biophys Biochem Cytol 1961;9:409–14.

[33] Langenkamp E, Vom Hagen FM, Zwiers PJ, Moorlag HE, Schouten JP, Hammes HP, et al. Tumor vascular morphology undergoes dramatic changes during outgrowth of B16 melanoma while proangiogenic gene expression remains unchanged. ISRN Oncol 2011;2011:409308.

[34] Colotta F, Allavena P, Sica A, Garlanda C, Mantovani A. Cancer-related inflammation, the seventh hallmark of cancer: links to genetic instability. Carcinogenesis 2009;30(7):1073–81.

[35] Bennett CM, Kanki JP, Rhodes J, Liu TX, Paw BH, Kieran MW, et al. Myelopoiesis in the zebrafish, Danio rerio. Blood 2001;98(3):643–51.

[36] Pearson RT, Warren NJ, Lewis AL, Armes SP, Battaglia G. Effect of pH and temperature on PMPC–PDPA copolymer self-assembly. Macromolecules 2013;46(4):1400–7.

[37] Prasmickaite L, BØ Engesæter, Skrbo N, Hellenes T, Kristian A, Oliver NK, et al. Aldehyde dehydrogenase (ALDH) activity does not select for cells with enhanced aggressive properties in malignant melanoma. PLoS ONE 2010;5(5):e10731.

[38] Weintraub A. All eyes on zebrafish. Lab Anim (NY) 2017;46(8):323–6.

[39] Geisler R, Köhler A, Dickmeis T, Strähle U. Archiving of zebrafish lines can reduce animal experiments in biomedical research. EMBO Rep 2017;18(1):1–2.

[40] Howe K, Clark MD, Torroja CF, Torrance J, Berthelot C, Muffato M, et al. The zebrafish reference genome sequence and its relationship to the human genome. Nature 2013;496(7446):498–503.

[41] Rajan V, Melong N, Wong WH, King B, Tong RS, Mahajan N, et al. Humanized zebrafish enhance human hematopoietic stem cell survival and promote acute myeloid leukemia clonal diversity. Haematologica 2019.

[42] Wehmas LC, Tanguay RL, Punnoose A, Greenwood JA. Developing a Novel Embryo-Larval Zebrafish Xenograft Assay to Prioritize Human Glioblastoma Therapeutics. Zebrafish 2016;13(4):317–29.

[43] Welker AM, Jaros BD, Puduvalli VK, Imitola J, Kaur B, Beattie CE. Standardized orthotopic xenografts in zebrafish reveal glioma cell-line-specific characteristics and tumor cell heterogeneity. Dis Model Mech 2016;9(2):199–210.

[44] Pudelko L, Edwards S, Balan M, Nyqvist D, Al-Saadi J, Dittmer J, et al. An orthotopic glioblastoma animal model suitable for high-throughput screenings. Neuro Oncol 2018;20(11):1475–84.

[45] Gaudenzi G, Albertelli M, Dicitore A, Wurth R, Gatto F, Barbieri F, et al. Patient-derived xenograft in zebrafish embryos: a new platform for translational research in neuroendocrine tumors. Endocrine 2017;57(2):214–9.

[46] Li Y, Jin K, van Pelt GW, van Dam H, Yu X, Mesker WE, et al. c-Myb enhances breast cancer invasion and metastasis through the Wnt/beta-Catenin/Axin2 pathway. Cancer Res 2016;76(11):3364–75.

[47] Dal N-JK, Kocere A, Wohlmann J, Van Herck S, Bauer TA, Resseguier J, et al. Zebrafish embryos allow prediction of nanoparticle circulation times in mice and facilitate quantification of nanoparticle–cell interactions. Small 2020;16(5):1906719.

[48] D'amico L, Seng WL, Yang Y, Suter W. Assessment of drug-induced cardiotoxicity in zebrafish. Zebrafish: P. McGrath (Ed.) 2011:45–54.

[49] Haldi M, Harden M, D'Amico L, DeLise A, Seng WL. Developmental toxicity assessment in zebrafish. In: McGrath P, editor. Zebrafish; 2011. p. 15–25.

[50] Vibe CB, Fenaroli F, Pires D, Wilson SR, Bogoeva V, Kalluru R, et al. Thioridazine in PLGA nanoparticles reduces toxicity and improves rifampicin therapy against mycobacterial infection in zebrafish. Nanotoxicology 2016;10(6):680–8.

[51] Jung DW, Oh ES, Park SH, Chang YT, Kim CH, Choi SY, et al. A novel zebrafish human tumor xenograft model validated for anti-cancer drug screening. Mol Biosyst 2012;8(7):1930–9.

[52] Yang J, Shimada Y, Olsthoorn RC, Snaar-Jagalska BE, Spaink HP, Kros A. Application of coiled coil peptides in liposomal anticancer drug delivery using a zebrafish xenograft model. ACS Nano 2016;10(8):7428–35.